

Effect of α -to- γ transformation on internal oxidation in FeCr-base alloys in dry and wet gases

Downloaded from: https://research.chalmers.se, 2025-11-11 00:17 UTC

Citation for the original published paper (version of record):

Chyrkin, A., Quadakkers, W. (2025). Effect of α-to-γ transformation on internal oxidation in FeCr-base alloys in dry and wet gases. Journal of Alloys and Compounds, 1045. http://dx.doi.org/10.1016/j.jallcom.2025.184722

N.B. When citing this work, cite the original published paper.

research.chalmers.se offers the possibility of retrieving research publications produced at Chalmers University of Technology. It covers all kind of research output: articles, dissertations, conference papers, reports etc. since 2004. research.chalmers.se is administrated and maintained by Chalmers Library

ELSEVIER

Contents lists available at ScienceDirect

Journal of Alloys and Compounds

journal homepage: www.elsevier.com/locate/jalcom



Effect of α -to- γ transformation on internal oxidation in FeCr-base alloys in dry and wet gases

Anton Chyrkin a,*, Willem Joseph Quadakkers b

- ^a Chalmers University of Technology, Department of Chemistry and Chemical Engineering, Kemivägen 10, Gothenburg 412 58, Sweden
- ^b Forschungszentrum Jülich GmbH, Institute for Energy Materials and Devices (IMD-1), Leo-Brandt-Straβe, Jülich 524 25, Germany

ARTICLE INFO

Keywords: Alloys Ferritic stainless steels Oxidation Ferrite Austenite

ABSTRACT

The transition from internal to external oxidation has been studied in ferritic and austenitic Fe-10Cr base model alloys in Fe/FeO Rhines pack and H_2/H_2O gas mixtures between 800 and 1100 °C. Ferritic and austenitic microstructures were stabilized by alloying with Mo (ferrite) and Ni (austenite), respectively. The α -to- γ transformation is experimentally demonstrated to be the primary trigger of internal oxidation in Fe-10Cr. Up to 1000 °C ferritic alloys can form external Cr_2O_3 scales while all austenitic alloys oxidized internally irrespective of the exposure environment. Wagnerian diffusion analysis accurately predicted the threshold of protectiveness (10 wt % at 1000°C) for the ferritic alloy as well as internal oxidation for the austenitic alloys. Water vapor promotes internal oxidation via increasing the effective oxygen permeability, i.e., the interfacial transport in the internal oxidation zone. However, the effect of H_2O and/or H_2 on the transition from external to internal oxidation is rather limited at 900 °C and above.

1. Introduction

Ferritic and ferritic/martensitic stainless steels comprise a separate family of steel grades based on the Fe-Cr system with Cr content varying from 10.5 to 29 wt% [1]. Ferritic steels find their application in various industries due to their corrosion and high temperature oxidation resistance as well as cost-effectiveness. They are commonly employed in automotive exhaust systems [2], in power plant boilers [3] and recently as a structural material for interconnects in solid-oxide fuel cells (SOFCs) [4–6] as well as solid-oxide electrolyzers (SOE) [7,8] and are often exposed to corrosive environments containing water vapor.

Ferritic stainless steels contain Cr contents of more than approximately $12\,\%$ and rely for oxidation resistance on the formation of a protective, well-adherend and slowly growing Cr_2O_3 -rich scale which forms on the alloy surfaces by selective oxidation of Cr during high-temperature exposure. Atmospheres containing water vapor are generally known to impede selective oxidation of Cr to form a continuous layer of Cr_2O_3 [9–13]. This effect is often related to a phenomenon termed breakaway oxidation, i.e., rapid oxidation of iron accompanied by internal oxidation of Cr. Breakaway oxidation is specifically relevant for Fe–Cr alloys with intermediate Cr contents (10–20 %). It is well-documented that alloys forming protective Cr_2O_3 -base scales in dry

gas such as air or oxygen may suffer from breakaway type oxidation in H_2O -containing gases. The oxidation rates in the wet gas may be three to five orders of magnitude higher than those in the dry gas [9,14,15].

The mechanisms of the detrimental water vapor effect on selective oxidation of high-temperature alloys have been lively debated in literature since the 1960s. Despite the substantial progress in this field, the understanding of the water vapor effect is far from being complete and satisfactory. The most well-understood and quantifiable phenomenon is volatilization of protective Cr₂O₃ in humid, high pO₂ gases [16-20] accelerating Cr-depletion from the alloy. Water vapor and hydrogen are also known to increase the growth rate of Cr_2O_3 in H_2/H_2O gas mixtures compared to that measured for the same materials exposed in dry air or oxygen [21-23]. Several mechanisms were proposed to explain the accelerated growth of Cr₂O₃ occurring in H₂/H₂O due to i) grain refinement in Cr₂O₃ [21], ii) gas-transport reactions via H₂/H₂O-bridges within in-scale voids [24], iii) incorporation of H⁺ or OH⁻ into the Cr₂O₃ [25,26]. Other mechanisms suggested explanations by iv) enhanced surface reaction and preferential adsorption of H2O molecules [10], v) enhanced growth stresses leading to oxide cracking resulting in enhanced consumption of Cr required for re-healing the scale [27].

All the afore-mentioned mechanisms assume that water vapor and/or hydrogen affect the transport of the involved species, primarily Cr and

E-mail address: chyrkin@chalmers.se (A. Chyrkin).

^{*} Corresponding author.

O, in the oxide scale or reactions at the gas-oxide interface. Another group of mechanisms suggest that hydrogen dissolved in the underlying alloy affects transport in the metal: oxygen permeability [14,28,29] and/or Cr at the alloy grain boundaries [30,31] (the latter being relevant only for low temperatures around 600 °C). The former mechanism was derived from studies in which a binary model alloy Fe-10Cr (wt%) showed external scale formation in Ar-O₂ but solely internal oxidation in Ar-4 %H₂-2 %H₂O [14]. A similar effect of hydrogen facilitating internal oxidation in Fe-Cr (5–10 wt%) alloys was reported by Ueda et al. [32, 33]. The oxygen permeability hypothesis strongly stimulated studies of internal oxidation in the past decade. The hydrogen effect on internal oxidation and oxygen permeability was questioned in a series of publications [34–40] demonstrating that this effect could neither be confirmed for the Fe-Ni-Cr system [34–36] in a broad range of concentration nor for binary Pd-Cr [40] and Fe-Cr [39] alloys.

The oxygen permeability hypothesis was finally revised in our previous publication [41] in which we studied the transition from external to internal oxidation in a binary Fe-10Cr alloy in the temperature interval 850–900 °C exposing the alloy to "dry" Fe/FeO Rhines pack and "humid" Ar-H₂-H₂O, constantly keeping the oxygen partial pressure (pO₂) at the level of FeO decomposition. Based on the thermodynamic and diffusion analysis, we hypothesized that the sharp transition from external Cr₂O₃ scaling to internal oxidation was primarily caused by the α -to- γ transformation occurring around 900 °C.

The aim of the present study is to

- experimentally verify the austenitization hypothesis introduced in [41] via alloying the initial Fe-10Cr alloy with Ni or Mo to stabilize the austenitic (face centered cubic, FCC) or ferritic (body centered cubic, BCC) alloy microstructures in a broader temperature interval, e.g., FCC at 800 °C and BCC at 900 °C and above.
- Differentiate between the α-to-γ transformation effect and the effect of water vapor on internal oxidation in Fe-Cr alloys.

2. Experimental procedure

2.1. Materials

The binary model alloy Fe-10Cr (wt%) and ternary model alloys Fe-10Cr-2Ni, Fe-10Cr-2Mo, Fe-10Cr-5Mo, and Fe-18Cr-2Mo (wt%) were supplied by MWH Hauner GmbH (Röttenbach, Germany). Pure metals of 99.995 % purity were arc-melted in vacuum. The chemical compositions of the alloys determined using Inductively Coupled Plasma Optical Emission Spectroscopy (ICP-OES) and Infrared Spectroscopy (IR) for C, S, N and O are listed in Table 1. The ingots were homogenized for 6 h at

Table 1
Chemical composition of the model alloys (in wt%) used in the present study measured by ICP-OES and IR spectroscopy.

	Fe-10Cr	Fe-10Cr- 2Ni	Fe-10Cr- 2Mo	Fe-10Cr- 5Mo	Fe-18Cr- 2Mo
Fe	Bal.	Bal.	Bal.	Bal.	Bal.
\mathbf{Cr}	9.98	10.42	10.21	10.3	18.32
Si	< 0.002	< 0.002	< 0.002	< 0.002	< 0.002
Al	0.011	0.009	0.0143	0.027	0.0157
Mn	0.0027	0.0002	< 0.001	0.0027	< 0.001
Ni	< 0.006	2.02	< 0.006	< 0.006	< 0.006
Mo	2.02	< 0.001	2.03	4.93	1.834
Nb	< 0.008	< 0.009	< 0.006	< 0.008	< 0.004
W	< 0.002	< 0.002	< 0.002	< 0.002	< 0.004
Ti	< 0.002	< 0.001	< 0.002	< 0.002	< 0.0007
Cu	< 0.003	< 0.003	< 0.002	< 0.003	< 0.004
Co	0.0061	0.0053	0.0058	0.0048	0.0017
Mg	< 0.002	< 0.002	< 0.002	< 0.002	< 0.001
P	< 0.008	< 0.009	< 0.008	< 0.007	< 0.007
C	0.010	0.010	0.010	0.013	0.010
N	0.005	0.005	0.005	0.005	0.004
0	0.018	0.025	0.021	0.019	0.061

 $1150~^\circ C$ in vacuum and subsequently hot-rolled to a 2.5 mm thick sheet. Test coupons measuring $20\times10\times2$ mm 3 were machined from the hot-rolled sheets. The average grain size of the alloys is approximately 50 μm for the ternary alloys and $10\,\mu m$ for Fe-10Cr. The specimen surfaces were polished with diamond paste to 0.25 μm surface finish. The specimens were degreased with acetone and ethanol in an ultrasonic bath and dried with pressurized air prior to exposure.

2.2. Rhines Pack exposures

The Fe/FeO Rhines pack (hereafter RP) [42] mixture was prepared from an iron powder supplied by BDH Chemicals Ltd (England) adopting a modified procedure described by Prillieux et al. [35]. The iron powder was oxidized in Ar-5H₂%-3 %H₂O at 800 °C for 24 h and dried in flowing argon at 200 °C for 5 h. The alloy coupons were put together with the Fe/FeO mixture in a 16 mm OD quartz tube and sealed under vacuum (10^{-5} mbar). The sealed quartz capsules were exposed in a horizontal tube furnace with a 4 cm wide stable hot zone at the envisaged temperature. The capsules were placed into a cold furnace and heated in stagnant air to the target temperature at 10 K per minute. After exposures the capsules were rapidly removed from the hot zone and subsequently cooled in air. The specimens were exposed at 800, 900, and 1000 °C for 72 h. Selected specimens were additionally exposed for 24 h at 1000 °C and 8 h at 1100°C.

2.3. H2/H2O exposures

The $\rm H_2/H_2O$ exposures were performed in an alumina tube in a horizontal furnace. The Ar-5 %H₂ gas mixture supplied by Linde Gas was bubbled through a humidifier kept at the envisaged temperature to obtain the gas humidity level, p(H₂O) in bar, corresponding to the Fe/FeO equilibrium (see gas compositions in Table 2). The alloy specimens were introduced into the cold furnace, flushed with the dry Ar-5 %H₂ gas for 1 h and heated at $10~\rm K~min^{-1}$ per minute to reach exposure temperature. The humidification was turned on once the furnace reached the target temperature. The cooling rate was $10~\rm K~min^{-1}$ as well. The gas flow rate was set at $200~\rm ml~min^{-1}$. The exposure temperatures and durations were the same as for the RP exposures.

2.4. Microstructural analyses

The exposed specimens were sectioned and milled using the broadion beam (BIB) technique employing a Leica EM TIC 3X. Selected specimens were hot-mounted in Polyfast resin (Struers, Denmark) to obtain the complete cross-section including the edges. The mounted specimens were mechanically ground to P1200 grit and polished with diamond pastes to $0.25\,\mu m$ surface finish. FEI Quanta 200 ESEM electron microscope equipped with an energy dispersive X-ray spectrometer (EDX) was used for post-exposure analyses.

Table 2 Partial pressures of oxygen, hydrogen and water vapor prevailing in exposures at the Fe/FeO equilibrium level at $800-1100^{\circ}$ C. Calculated using standard enthalpies and entropies from [78].

Exposure temperature	pO ₂ in Fe/FeO [bar]	pH ₂ [mbar]	pH ₂ O [mbar]	pO_2 in H_2/H_2O [bar]	Dew point [°C]
800	1.1×10^{-19}	49	22	1.1×10^{-19}	19.0
900	1.7×10^{-17}	49	26	1.7×10^{-17}	21.7
1000	1.2×10^{-15}	49	30	1.2×10^{-15}	24.4
1100	4.7×10^{-14}	49	35	4.6×10^{-14}	26.7

3. Results

3.1. Oxidation morphologies

3.1.1. Fe-10Cr

Fig. 1 shows the BSE SEM micrographs of the cross-sectioned Fe-10Cr specimens exposed in Fe/FeO RP and the $\rm H_2/H_2O$ gas mixture for $72\,h$ at 800, 900, and 1000 °C. At 800 °C, Fe-10Cr grows external $\rm Cr_2O_3$ scales in both RP and $\rm H_2/H_2O$. In $\rm H_2/H_2O$, however, the external oxide scale is accompanied by intergranular internal oxidation attack. Similar oxide scale microstructures were reported by Zurek et al. [43] and recently also for Fe-10Cr at 850 °C [41]. The internal oxides are reported to be spinel of the (Fe,Cr)_3O_4 type. At 900 and 1000 °C, the situation is fundamentally different: Fe-10Cr oxidizes fully internally in both environments. The internal oxidation zone (IOZ) is slightly deeper in $\rm H_2/H_2O$ compared to the RP specimen in agreement with previous findings for this alloy at 900 °C [41] and for Fe-5Cr at 800 °C [32,33]

3.1.2. Fe-10Cr-2Ni

Fig. 2 shows the BSE SEM micrographs of the cross-sectioned Fe-10Cr-2Ni after 72 h exposure in $\rm H_2/H_2O$ and RP at 800 and 900 °C. In contrast to unalloyed binary Fe-10Cr, Fe-10Cr-2Ni exhibits full internal oxidation at 800 °C (compare Fig. 2a,b with Fig. 1a,b) irrespective of the exposure atmosphere. Alloying with 2 wt% Ni clearly promoted internal oxidation. At 900 °C, the depths of the IOZs in Fe-10Cr and Fe-10Cr-2Ni hardly differed (38.5 μm in $\rm H_2/H_2O$ and 36.2 μm in RP). Although alloying with Ni is known to dramatically reduce oxygen permeability in iron [34,36], alloying with 2 wt% only had a very limited effect on the internal oxidation kinetics. The Ni-alloyed Fe-10Cr demonstrated exclusive internal oxidation at 800–900 °C.

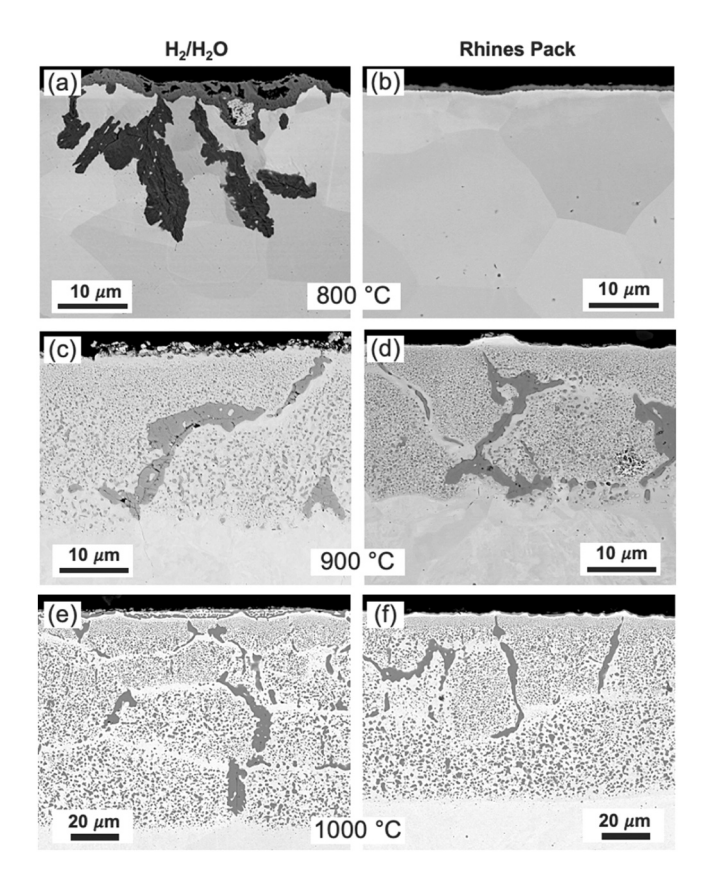


Fig. 1. BSE images of cross-sectioned Fe-10Cr alloy specimens exposed for 72 h at 800, 900, and 1000 $^{\circ}$ C in (a,c,e) H₂/H₂O, gas compositions in Table 2, and (b, d,f) Fe/FeO RP.

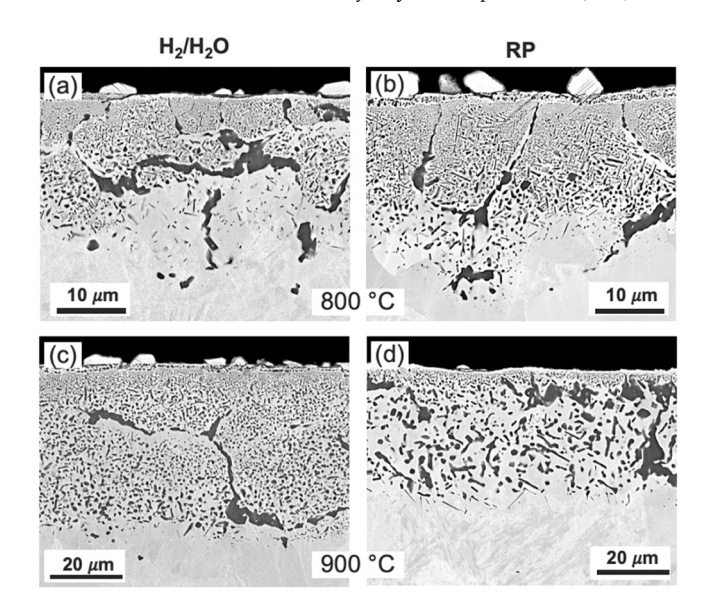


Fig. 2. BSE images of cross-sectioned Fe-10Cr-2Ni alloy specimens exposed for 72 h at 800 and 900 $^{\circ}$ C in (a,c) H₂/H₂O, gas compositions listed in Table 2, and (b,d) Fe/FeO RP.

3.1.3. Fe-10Cr-2Mo

Fig. 3 shows the BSE SEM micrographs of the cross-sectioned Fe-10Cr-2Mo after 72 h exposure in $\rm H_2/H_2O$ and RP at 900 and 1000 °C. Alloying with Mo had a clearly pronounced beneficial effect on external oxidation. Unlike binary Fe-10Cr at 900 °C (Fig. 1c,d), Fe-10Cr-2Mo grew an external $\rm Cr_2O_3$ scale in both $\rm H_2/H_2O$ and RP, the scale being thicker in $\rm H_2/H_2O$ (5.1 μm) than in RP (3.1 μm). At 1000 °C, the situation is again different compared to 900 °C: Fe-10Cr-2Mo oxidized internally in both exposure atmospheres. Similar to Fe-10Cr, the IOZ in $\rm H_2/H_2O$ is slightly deeper than that in RP. Interestingly, Fe-10Cr-2Mo oxidized in RP formed an external oxide layer over the IOZ. The EDX analysis showed that this oxide layer contained both Cr and Fe. In other words, the Fe-10Cr-2Mo specimen exposed in RP at 1000 °C managed to grow an external $\rm Cr_2O_3$ scale, which eventually lost protectiveness and transformed into Fe-rich spinel.

In contrast to the RP specimen (Fig. 3b), the specimen exposed in H₂/

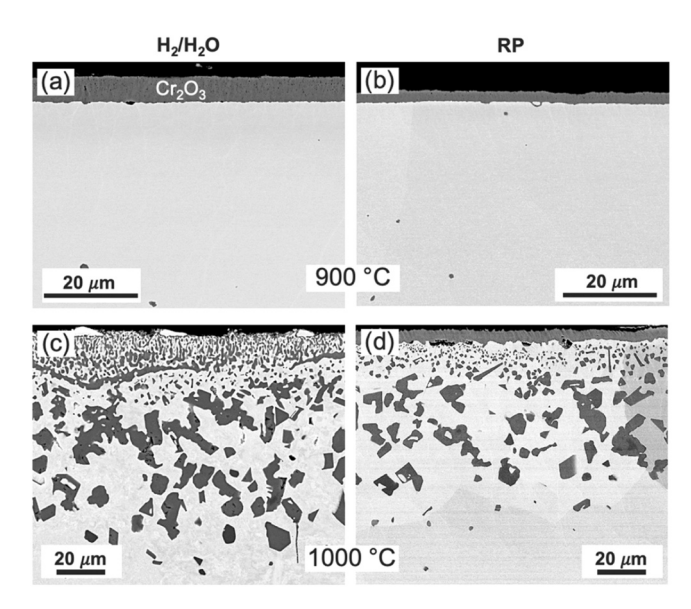


Fig. 3. BSE images of cross-sectioned Fe-10Cr-2Mo alloy specimens exposed for 72 h at 900 and 1000 $^{\circ}$ C in (a,c) H₂/H₂O, gas compositions listed in Table 2, and (b,d) Fe/FeO RP.

 $\rm H_2O$ at 1000 °C (Fig. 3b) had metal extrusions on the surface, which is indicative of fully internal oxidation from the very early stages of the exposure.

The big difference in oxidation behavior of Fe-10Cr-2Mo between 900 and 1000 $^{\circ}\text{C}$ is similar to that observed for Fe-10Cr between 800 and 900 $^{\circ}\text{C}$ (Fig. 1). The latter is believed to be triggered by the $\alpha\text{-to-}\gamma$ transformation occurring above 850 $^{\circ}\text{C}$. Fe-10Cr-2Mo is fully ferric (BCC) at 1000 $^{\circ}\text{C}$ (see Fig. 7), however, the alloy composition is very close to the $\gamma\text{-loop}$. Therefore, a very minor Cr depletion may induce the $\alpha\text{-to-}\gamma$ transformation in the subsurface of Fe-10Cr-2Mo.

3.2. Austenitization at 1000 °C

To quantitatively estimate the Cr-depletion in Fe-10Cr-2Mo due to external scale formation, subscale Cr concentration profiles shown in Fig. 4 were measured with EDX after exposure at 900 °C in both RP and $\rm H_2/H_2O$. The Cr profile obtained in $\rm H_2/H_2O$ is steeper than that in the RP specimen which agrees with the oxide thickness measurements (Fig. 3a, b). The Cr depletion at the oxide-metal interface amounts to 2 wt% in RP and to 5 wt% in $\rm H_2/H_2O$, respectively. According to the phase diagram in Fig. 7, a 2 wt% Cr depletion (Fe-8Cr in the diagram) is sufficient to start forming FCC while 5 % (Fe-5Cr in the diagram) is enough for a complete austenitization.

To verify this assumption, the concentration of Mo in the ternary model alloy was increased to 5 wt%. According to the Fe-Mo phase diagram [44], the Fe-5Mo alloy is fully ferritic (BCC) between 800 and 1200 °C. Fig. 5 demonstrates BSE micrographs of the cross-sectioned Fe-10Cr-5Mo after 72 h exposure in $\rm H_2/H_2O$ and RP at 900 and 1000 °C. At both temperatures, Fe-10Cr-5Mo is capable of growing external $\rm Cr_2O_3$ irrespective of the exposure environment.

3.3. Temperature dependence

Chemical failure of the $\rm Cr_2O_3$ scale thermally grown on a ferritic Fe-10Cr base alloy can be further explored once the ferritic structure is stabilized in the model alloy Fe-10Cr-5Mo over a broad temperature range (Fig. 5). Fig. 6 shows BSE SEM images of the cross-sectioned specimens of alloy Fe-10Cr-5Mo exposed at 900 °C, 1000 °C, and 1100 °C in Fe/FeO RP and $\rm H_2/H_2O$ gas mixtures. The images were taken at the edges of the cross-sectioned specimens while the high-magnification insets display the oxide scales grown on the flat surface

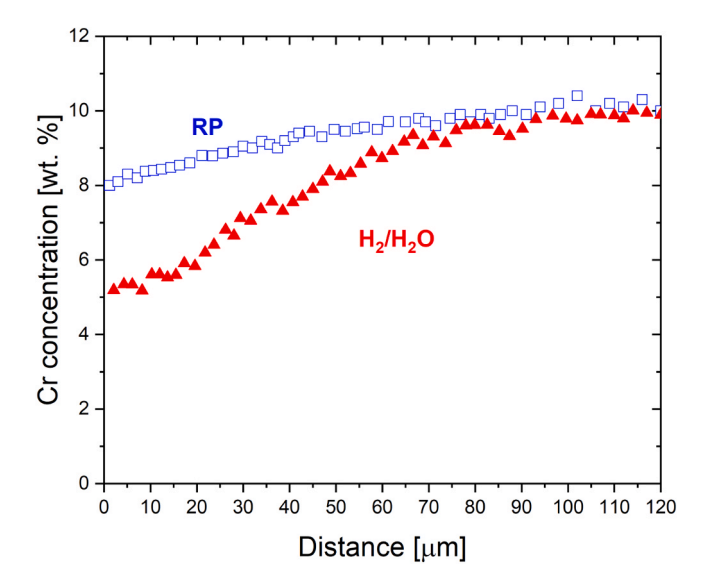


Fig. 4. Cr concentration profiles beneath the external $\rm Cr_2O_3$ scales measured by EDX in Fe-10Cr-2Mo after 72 h oxidation in Fe/FeO Rhines pack (RP) and $\rm H_2/H_2O$ gas mixture at 900 °C.

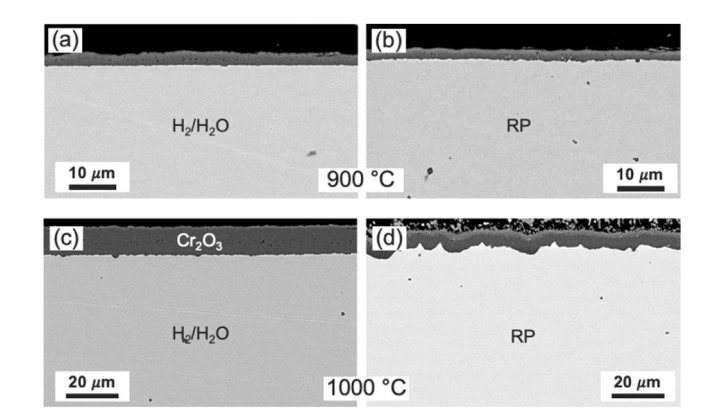


Fig. 5. BSE images of cross-sectioned Fe-10Cr-5Mo alloy specimens exposed for 72 h at 900 and 1000 $^{\circ}$ C in (a,c) $\rm H_2/H_2O$, gas compositions listed in Table 2, and (b,d) Fe/FeO RP.

in the middle of the specimen. At 900 °C and 1000 °C, Fe-10Cr-5Mo formed protective external Cr_2O_3 scales in both exposure environments. At 1100 °C, the corners of the specimens are attacked by internal oxidation in both atmospheres, the effect being most pronounced in H_2/H_2O . The transition between external and internal oxidation in ferritic Fe-10Cr-5Mo must have occurred between 1000 and 1100 °C.

To quantify the transition from protective (external) to unprotective (internal) oxidation, Cr-depletion at the oxide-metal interface was measured for all the exposed specimens able to grow external Cr_2O_3 including the reference alloy Fe-18Cr-2Mo (protective in all studied conditions) exposed in parallel in all experiments. Table 3 summarizes the Cr-depletion values derived from the Cr-concentration profiles measured by EDX as demonstrated e.g. in (Fig. 4). The values of Cr-depletion at the oxide-alloy interface show virtually no temperature dependence and are higher for H_2/H_2O (5.0 \pm 0.3 wt%) compared to RP (2.2 \pm 0.3 wt%) due to a higher chromia scaling rate in H_2/H_2O .

4. Discussion

4.1. Austenitization hypothesis

In our previous publication [41], we suggested that the α -to- γ transformation is the main trigger of internal oxidation in a binary alloy Fe-10Cr at 900 °C. Water vapor/hydrogen was found to promote internal oxidation via higher oxygen uptakes resulting in deeper IOZs. However, this effect was rather limited compared to the dramatic changes of the kinetic parameters such as oxygen permeability and Cr diffusivity produced by austenitization as predicted by the Fe-Cr phase diagram [45]. The classical Wagnerian diffusion analysis [46,47] for Fe-10Cr in [41] predicted external scaling for BCC at 800–900 °C and internal oxidation in FCC in a broad temperature interval of 600–1200 °C. Alloying Fe-10Cr with elements stabilizing a certain lattice, e.g. Ni for FCC and Mo for BCC, helped validate this prediction.

Fig. 7 shows a segment of the binary Fe-Cr phase diagram calculated in Thermo-Calc using the TCFE6 Steel database [48]. The phase diagram calculation was mapped to cover primarily the γ -loop in the Fe-Cr system. Quasi-binary sections for Fe-Cr-2Mo and Fe-Cr-2Ni (wt%) were calculated using the same approach and superimposed on the binary phase diagrams in Fig. 7a,b.

A binary alloy Fe-10Cr is predicted to be fully ferritic (BCC) at 800 °C and fully austenitic at 900 °C and 1000 °C. Alloying with 2 % Mo significantly compresses the γ -loop so that the alloy Fe-10Cr-2Mo is predicted to be completely ferritic (BBC) throughout the entire range of Cr concentration at 900 °C (Fig. 7b). The alloy is ferritic also at 1000 °C, however, it is very close to the γ -loop. Therefore, a minor Cr-depletion due to oxidation may result in the α -to- γ transformation. On the other hand, alloying with 2 % Ni expands the γ -field so that the composition

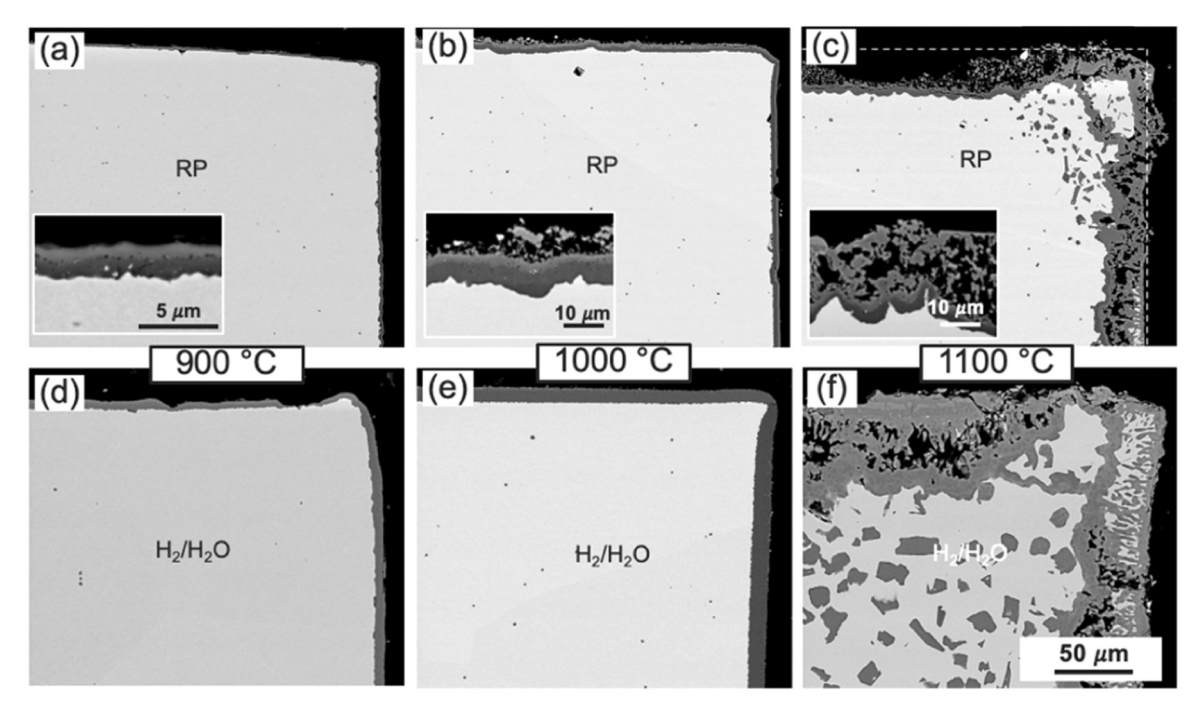


Fig. 6. BSE images of cross-sectioned Fe-10Cr-5Mo alloy specimens exposed for 72 h at 900 °C (a,d), 24 h at 1000 °C (b,e), and 8 h at 1100 °C (c,f) in (a,b,c) Fe/FeO RP and (d,e,f) H₂/H₂O, gas compositions listed in Table 2. Images were taken in the specimen corner. Inserted figures were taken from the flat part of the specimens.

Table 3

Cr concentration at the oxide-alloy interface in wt% measured by EDX for the alloys used in the present study that formed external $\rm Cr_2O_3$ scales on Fe-10Cr-2Mo, Fe-18Cr-2Mo and Fe-10Cr-5Mo. The alloy specimens were exposed for 72 h at 800 °C, 72 h at 900 °C, 24 h at 1000 °C, 8 h at 1100 °C in $\rm H_2/H_2O$ and RP. Cr depletion was calculated as the difference between the bulk concentration of Cr, $\rm C^0_{Cr}$, and the Cr concentration at the oxide-alloy interface, $\rm C^{int}_{Cr}$. Oxide thickness, $\rm X_{ox}$, was measured in the SEM images. The measurement error for Cr concentration was 0.3 wt% while the error for oxide thickness measurement was 0.2 $\rm cm$

	Fe/FeO Rhines pack			H ₂ /H ₂ O			
Alloy	X _{ox} μm]	C ^{int} [wt%]	$C_{Cr}^0 - C_{Cr}^{int}$ [wt%]	X _{ox} μm]	C ^{int} [wt%]	$C_{Cr}^0 - C_{Cr}^{int}$ [wt%]	
	800 °C						
Fe-18Cr-2Mo	1.9	14.3	3.7	2.6	13.5	4.5	
	900°	С	10.0				
Fe-10Cr-2Mo	4.3	8.0	2.2	8.2	5.1	5.1	
Fe-10Cr-5Mo	4.0	8.2	2.1	8.4	5.0	5.5	
Fe-18Cr-2Mo	4.2	16.1	2.2	8.4	13.0	5.3	
	1000	°C			13.0		
Fe-10Cr-5Mo	5.3	8.5	1.8	9.6	5.7	4.6	
Fe-18Cr-2Mo	5.2	16.4	1.9	9.8	13.6	13.6	
	1100	°C					
Fe-18Cr-2Mo	6.0	15.8	2.5	10.9	13.2	5.1	

Fe-10Cr-2Ni is fully austenitic (FCC) at both 800 and 900 °C (Fig. 7b). Providing that the austenitization hypothesis [41] is correct, i.e., ferritic Fe-10Cr oxidizes externally while austenitic Fe-10Cr is prone to internal oxidation at 800–900 °C, alloy Fe-10Cr-2Mo should produce an external $\rm Cr_2O_3$ scale at 900 °C while the unalloyed binary (austenitic) Fe-10Cr will oxidize internally. Vice versa, alloy Fe-10Cr-2Ni will oxidize internally while the unalloyed (ferritic) Fe-10Cr will grow external $\rm Cr_2O_3$ at 800 °C. This hypothesis was experimentally verified in

the present study. Stabilizing BCC via alloying with Mo promoted external scaling at 900 °C (Fig. 3a,b) and even 1000 °C (Fig. 5) while stabilizing FCC with Ni resulted in the opposite, i.e., internal oxidation (Fig. 2). The effect of the lattice on the oxidation pattern of Fe-10Cr at 800-1000 °C is very clear and will in the next section be quantified using the classical diffusion analysis introduced by Carl Wagner [46,47,49].

4.2. Diffusion analysis for BCC

Carl Wagner developed a mathematical approach to describe internal [46] and external [47,49] oxidation of a binary alloy A-B in which B reacts with oxygen and A remains inert. These models are based on equating competing fluxes: i) ingress of oxygen vs counter-diffusion of the scale-forming element B and ii) consumption of B by the growing external oxide vs supply of this element from the alloy via diffusion. These predictive tools are often used to interpret breakaway oxidation of FeCr- and NiCr-base alloys [14,50,51].

Wagner elaborated two fundamental criteria for the formation and maintenance of a protective external oxide scale. The first criterion predicts the minimum concentration of B (Cr in the present study) required to overcome the inward ingress of oxygen dissolved in the metal by counter-diffusion of B preventing thereby internal oxidation. $N_R^{crit.1}$ is given by

$$N_B^{crit,1} > \left[\frac{\pi g^*}{3} \frac{\overline{V}_m}{\overline{V}ox} \frac{N_O^{(s)} D_O}{\widetilde{D}_R} \right]^{\frac{1}{2}} \tag{1}$$

where $N_O^{(s)}$ is the oxygen solubility in the alloy in terms of mole-fraction, D_O is the diffusivity of oxygen in m^2 s⁻¹, \widetilde{D}_B is the interdiffusion coefficient of B in the alloy in m^2 s⁻¹, \overline{V}_m and $\overline{V}ox$ are the molar volumes of the alloy and oxide in m^3 mol⁻¹, respectively. The internal oxide in the Fe-Cr system is chromia, thus, the \overline{V}_m and $\overline{V}ox$ are 7×10^{-6} and 15×10^{-6} m³ mol⁻¹, respectively. The factor g^* is postulated as the minimum volume-fraction of internal oxide to induce the transition from internal to external oxidation and has been approximated by Rapp [52] as 0.3.

The second Wagnerian criterion predicts the minimum alloy con-

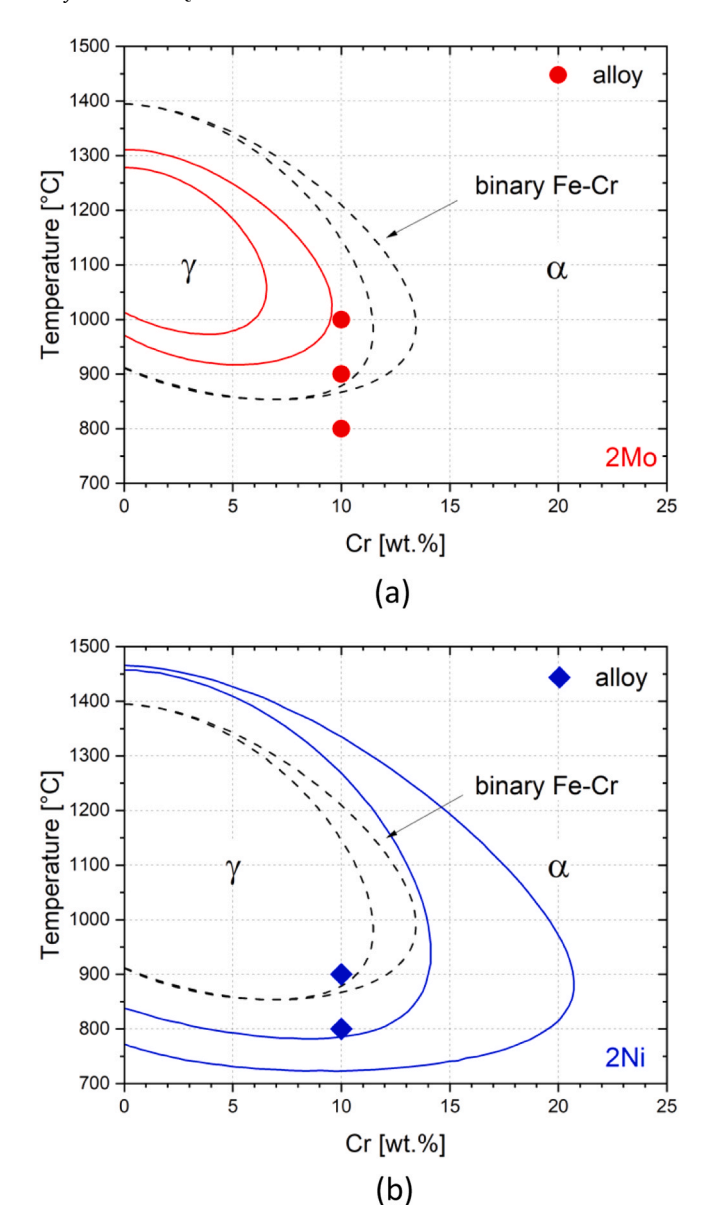


Fig. 7. Fragment of binary Fe-Cr phase diagram demonstrating effects of alloying Fe-Cr with 2 wt% Mo (a) and 2 wt% Ni (b) on the $\gamma\text{-loop}$ (black dashed lines) calculated in Thermo-Calc using TCFE9 database. Symbols denote the alloy Fe-10Cr-2X (X = Mo, Ni) at test temperatures of 800 °C, 900 °C, and 1000 °C.

centration of B, $N_B^{crit,2}$, to sustain the protective oxide scale once it has been formed on the surface. The second criterion can be expressed as

$$N_B^{crit,2} > \left(\frac{\pi k_c}{2\widetilde{D}_B}\right)^{\frac{1}{2}}$$
 (2)

where k_c is the parabolic rate constant in terms of metal recession in m² s⁻¹.

The input data for the calculation of $N_{Cr}^{crit,1}$ and $N_{Cr}^{crit,2}$ for BCC and FCC are tabulated along with the calculated values in Table 4. The calculated values of the critical Cr concentrations are graphically presented in Fig. 8. The oxygen solubility and diffusivity data are taken from [53], Cr diffusion coefficients were taken from [54] for BCC and from [55] for FCC. Oxidation rates were metallographically determined by measuring oxide thickness in the SEM images (see e.g. Fig. 5 and Table 3).

The $N_{Cr}^{crit,1}$ values for ferrite (BCC) are identical with the calculations in [14,41], increase with increasing temperature and predict external oxidation for ferritic Fe-10Cr below 1000 °C. Eq. (1) accurately

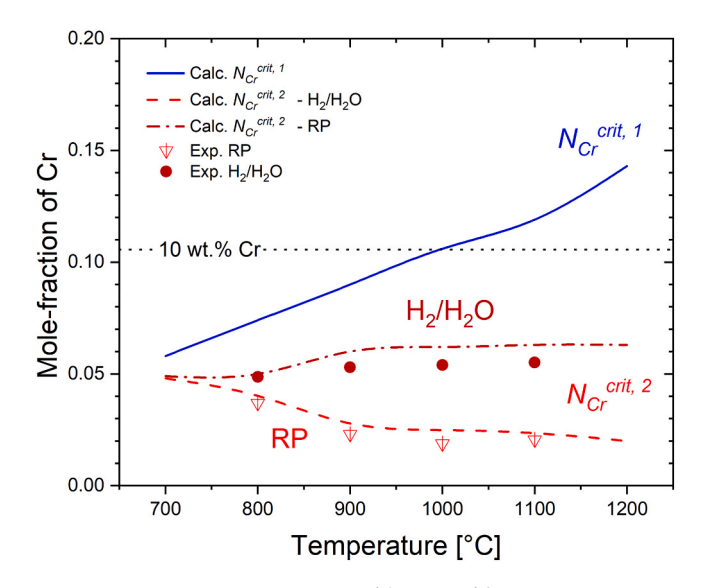


Fig. 8. Temperature dependence of $N_{Cr}^{crit,1}$ and $N_{Cr}^{crit,2}$ calculated for binary ferritic alloy system Fe-Cr using Eqs. (1) and (2), respectively. The input parameters along with the data sources are summarized in Table 4. The experimental measurements for $N_{Cr}^{crit,2}$ (empty triangles for RP and full circles for H_2 O) are Cr-depletion values measured at the oxide-metal interface in the exposed specimens (see also Table 3). The experimental values of Cr-depletion were measured with EDX in Fe-10Cr-2Mo, Fe-18Cr-2Mo and Fe-10Cr-5Mo after exposures in RP and H_2/H_2 O at 800, 900, 1000 and 1100 °C.

Table 4
Calculated $N_{Cr}^{crit.1}$ and $N_{Cr}^{crit.2}$ for ferritic (BCC) and austenitic (FCC) binary Fe-Cr system at 800–1100 °C along with the literature data used for calculation. The oxygen solubility and diffusivity data were taken from [53], Cr diffusion coefficients were taken from [54] for BCC and from [55] for FCC. Oxidation rates were determined from oxide thickness in SEM images.

T [°C]	$N_O^{(s)}$	$[\mathrm{m}^2\mathrm{s}^{-1}]$	\widetilde{D}_{Cr} $[\mathrm{m}^2\mathrm{s}^{-1}]$	k_c RP $[\mathrm{m}^2\mathrm{s}^{-1}]$	k_c H_2/H_2O $[m^2s^{-1}]$	$N_{Cr}^{crit,1}$	$N_{Cr}^{crit,2}$ RP	$N_{Cr}^{crit,2}$ H_2/H_2O		
Ferrite (BCC	Ferrite (BCC)									
800	1.6×10^{-6}	1.0×10^{-10}	3.0×10^{-15}	1.7×10^{-18}	3.2×10^{-18}	0.089	0.024	0.031		
900	$3.0 imes 10^{-6}$	1.7×10^{-10}	9.0×10^{-15}	6.4×10^{-18}	3.0×10^{-17}	0.093	0,027	0.057		
1000	$8.3 imes 10^{-6}$	3.7×10^{-10}	1.5×10^{-14}	8.4×10^{-18}	5.3×10^{-17}	0.110	0.024	0.059		
1100	2.0×10^{-5}	7.3×10^{-10}	1.5×10^{-13}	1.7×10^{-16}	5.1×10^{-16}	0.125	0.033	0.059		
Austenite (F	FCC)									
800	3.1×10^{-6}	3.5×10^{-12}	2.9×10^{-17}	1.7×10^{-18}	3.2×10^{-18}	0.230	0.306	0.420		
900	6.8×10^{-6}	1.8×10^{-11}	3.0×10^{-16}	8.4×10^{-18}	3.0×10^{-17}	0.241	0.183	0.397		
1000	$1.3 imes 10^{-5}$	6.7×10^{-11}	2.2×10^{-15}	3.3×10^{-17}	1.3×10^{-16}	0.248	0.12	0.196		
1100	2.4×10^{-5}	2.2×10^{-10}	1.2×10^{-14}	1.9×10^{-16}	5.9×10^{-16}	0.259	0.10	0.181		

predicted the threshold of protective scaling of 10 wt% for BCC as Fe-10Cr-5Mo showed signs of internal oxidation at 1100 °C in both RP and $\rm H_2/H_2O$. For austenitic Fe-10Cr, the situation is dramatically different because $N_{Cr}^{crit,1}$ is very much above 10 wt% in the entire temperature range of 800–1100 °C. This prediction agrees with the observations for austenitic Fe-10Cr-2Ni at 800 °C (Fig. 2, compare with ferritic Fe-10Cr at 800 °C in Fig. 1) and Fe-10Cr at 900 °C and above (austenitic above 900 °C, see Fig. 7) and even initially ferritic Fe-10Cr-2Mo (Fig. 3 and Fig. 7) which transforms into austenite due to Cr-depletion as a result of external chromia formation (Fig. 4).

Experimental validation of criterion $N_{Cr}^{crit,1}$ for Fe-Cr is not an easy task. I would require a set of model alloys to map the critical Cr concentration as a function of temperature as well as controlling the α -to- γ transformation via proper alloying tactics. Elements such as Ti, Nb and Si are known to stabilize the ferritic microstructure [56] and thus extend the chemical lifetime of ferritic stainless steels [57]. However, their addition to Fe-Cr would significantly affect the oxide composition and thus the oxidation kinetics and therefore would affect $N_{Cr}^{crit,2}$. At the same time, $N_{Cr}^{crit,2}$ is directly measurable. According to Wagner's theory [47], the Cr concentration at the interface between the alloy and the external chromia scale is time-independent and can be expressed as

$$N_B^{\text{int}} = N_B^0 - \left(\frac{\pi k_c}{2\widetilde{D}_B}\right)^{\frac{1}{2}} \tag{3}$$

Combining Eqs. (2) and (3) and assuming a limiting case of full depletion ($N_B^{\rm int}=0$), the experimentally measurable Cr depletion equals $N_B^0-N_B^{\rm int}=N_{Cr}^{\rm crit.2}$. The measured Cr-depletion values summarized in Table 3 agree very well with the calculated $N_{Cr}^{\rm crit.2}$ values for BCC in Table 4: e.g. an averaged value of 2.2 ± 0.3 wt% for RP and 5.0 ± 0.3 wt% for H₂/H₂O at 900 °C. Unlike $N_{Cr}^{\rm crit.1}$, the temperature dependence of $N_{Cr}^{\rm crit.2}$ for BCC is rather weak presumably due to an only minor difference in activation energies for Cr_2O_3 growth and Cr diffusion in ferrite as discussed in detail in [41].

The accuracy of predicting of $N_{Cr}^{crit,1}$ and $N_{Cr}^{crit,2}$ for austenite cannot be concluded from the present experimental results because i) all alloys which demonstrated external scaling were ferritic and ii) 10 wt% is too low for exploring these kinetic boundaries. A minimum concentration of 18 wt% has been empirically derived for austenitic steels and is the lowest level of Cr in the commercially available austenitic steel grades [58].

The Wagnerian diffusion analysis leads to three important conclusions:

- The transition from external to internal oxidation of Fe-10Cr at 900 °C and above in both RP and H_2/H_2O is predominantly governed by the alloy microstructure. The failure of the external Cr_2O_3 scale on ferritic alloys is driven by the oxidation-induced α -to- γ phase transformation. Ferritic Fe-10Cr can grow external Cr_2O_3 up to 1000 °C (both $N_{Cr}^{crit,1}$ and $N_{Cr}^{crit,2}$ are fulfilled). Austenitic Fe-10Cr is predicted to oxidize internally ($N_{Cr}^{crit,1}$ and $N_{Cr}^{crit,2}$ significantly exceed 10 wt%) in the entire temperature range of 800–1100 °C.
- Wagner's models very accurately predict a) transition from internal to external oxidation for the ferritic Fe-Cr system around 1000 °C and b) the extent of interfacial Cr-depletion with respect to the exposure environment (different k_c values for RP and H₂/H₂O).
- Water vapor/hydrogen is not the main factor governing the transition from internal to external oxidation of FeCr-base alloys above 900 °C

4.3. Effect of water vapor

Water vapor is well-known to deteriorate the protective oxidation of FeCr-base alloys in humid high-pO $_2$ gases such as air [10,11,18,19,59]

or oxyfuel gas [59,60], steam [61–63], reducing H_2/H_2O gases [12,13,64,65] and dual-atmosphere conditions [66–69]. The main well-understood failure mechanism discussed in literature is reactive evaporation of volatile Cr-species [16,18–20,70] in water vapor containing high-pO₂ gases. The Cr evaporation effect is well quantifiable while multiple coating systems have been proposed to mitigate this effect e.g. in SOFCs/SOECs [70–72].

Other mechanisms such as i) preferential adsorption of H_2O [10], ii) H_2/H_2O -briges promoting gas-transport reactions within voids in the oxide scale [24], iii) acceleration of Cr_2O_3 growth via proton doping [25,26] or grain refinement in the Cr_2O_3 scale [21] usually describe a specific case and cannot be generally applied to all exposure conditions and alloy systems. In the present study, Cr-vaporization is irrelevant due to the low PO_2 . The mechanisms (ii) and (iii) may be viewed as one mechanism of accelerated Cr_2O_3 growth in H_2/H_2O .

Another important mechanism that has been debated in literature in the past 15 years is the enhancement of internal oxidation and oxygen permeability due to presence of water vapor/hydrogen. This hypothesis was first introduced in a series of publications by Essuman et al. [14,28, 29,50]. The idea was supported by independent experimental evidence [32,33] also observed in [41] and in the present work: IOZs in binary Fe-Cr alloys are somewhat (10–15 %) deeper in the humid environments (see Fig. 1c-f) compared to "dry" RP. In the original studies [14,28,29,50], it was proposed that hydrogen dissolved in the alloy increased oxygen permeability via extending the lattice. This hypothesis was questioned in multiple studies for Fe-Ni-Cr [34–36], Pd-Cr [38,40] and binary Fe-Cr [39] which demonstrated that in various alloy systems lattice oxygen permeability is not affected by water vapor/hydrogen.

At the same time, experimental evidence [32,33,41] including the present study suggests that humidity does facilitate internal oxidation and thus unprotective corrosion behavior, especially at lower temperatures e.g. 500-700 °C [9,12,13]. It should be mentioned that the experiments with Fe-10Cr in RP and H₂/H₂O [32,33,41] can be perceived as misleading with respect to the oxygen permeability hypothesis. Indeed, the IOZs are wider in humid gases [33,41] in highly alloyed binary alloys (e.g. 10 wt%) while the IOZs measured in diluted (0.5–2 % Cr) are equally thick for dry and humid exposures [39].

The increase in IOZ depth and herewith the increase of apparent oxygen permeability due to presence of H_2O/H_2 has unequivocally been demonstrated in case of Fe-10Cr in the present study and e.g. in references [32,33,41], however it is easy to derive from Eq. (1) that this effect only results in a very minor increase of $N_B^{crit,1}$ from 0.093 to only 0.101 at 900 °C. Thicker IOZs in H_2/H_2O are most likely related to the accelerated oxygen transport along the incoherent oxide-metal interfaces in the IOZ as described in [33]. The dependency of apparent oxygen permeability on Cr concentration was expressed as:

$$\left[N_O^{(s)}D_O\right] = \left[N_O^{(s)}D_O\right]_{lattice} + BN_{Cr} \tag{4}$$

where B is an empirical constant, i.e., the experimentally measured slope of the oxygen permeability dependence on Cr concentration. The model was derived based on the studies of internal oxidation morphologies [73–75] while the ratio $\frac{B_{humid}}{B_{dry}}$ was termed as the enhancement factor f_E . The enhancement factor measured in [33] was 1.2 which agrees well with the present study.

The enhanced transport of oxygen along the incoherent oxide-metal interfaces in humid gases clearly is not the crucial factor which is responsible for the change from external to internal Cr oxidation in wet gas at 900 °C as demonstrated in the present work and [32,33,41]. However, the situation may significantly change at lower temperatures e.g. 600–650 °C where the difference in corrosion behavior between dry and water vapor containing gases is more pronounced than at higher temperatures [12,30,31,64]. At lower temperatures, the flux balancing in Eq. (1) must include the grain-boundary (GB) transport contributions which are difficult to quantify based on the available data. Multiple

experimental observations [12,13] demonstrate that for Fe-Cr at 600–650 °C in humid gases $N_{Cr}^{crit,1}$ is in the range of 0.25 – 0.30 while Eq. (1) using bulk transport parameter predicts 0.05. Thus, the overall enhancement factor f_E must be at least 25 to accommodate this change of Cr and/or O transport, which is significantly higher than experimentally measured values at 800–900 °C. Dedicated experiments are required to quantify the GB transport contributions of the corresponding oxygen and chromium fluxes in Eq. (1) to correctly evaluate the effect of water vapor and/or hydrogen on $N_{Cr}^{crit,1}$. The latter is challenging but seems to be realistic as the Wagnerian equations correctly predict $N_{Cr}^{crit,1}$ and $N_{Cr}^{crit,2}$ at higher temperatures with the dominating lattice transport and the minor contribution of oxygen transport along metal/oxide interface boundaries.

Finally, water vapor is also known to affect the critical oxide volume g^* in Eq. (1) [76,77] by affecting the precipitate morphology as demonstrated to be extremely relevant for needle-like precipitates frequently occurring in binary Ni-Al alloys. However, this morphological effect is rather weak in the Fe-Cr system. Furthermore, big changes (factor of 25 as demonstrated above) of g^* are difficult to imagine as the critical oxide volume-fraction varies from zero to unity while the resulting enhancement factor is additionally square-rooted in Eq. (1). The increase in g^* factor can thus hardly explain the increase of $N_{Cr}^{crit,1}$ from 0.05 to 0.25 at 600–650 °C in humid gases as demonstrated e.g. in [12,13]

Although the initial oxygen permeability hypothesis can be considered disproved, a corrected internal oxidation hypothesis can be repostulated:

- The lattice oxygen permeability, $N_O^{(s)}D_O$, is not affected by water vapor or hydrogen irrespective of base-metal (Fe, Ni, Pd, etc.).
- In contrast to bulk permeability, the overall apparent oxygen permeability governed by GB transport and precipitate morphology in the IOZ is affected by water vapor and seems to be especially of significance at lower temperatures.

In the present work, the H_2/H_2O effect on internal oxidation is observed (Fig. 1), but it is much weaker compared to the effect of the α -to- γ transformation on oxidation. For binary ferritic Fe-10Cr at 800 °C, exposure in H_2/H_2O resulted in internal oxidation attack underneath the external Cr_2O_3 scale, whereas this did not occur during RP exposure. For austenitic alloys, the IOZs are slightly deeper after the exposures in H_2/H_2O compared to RP (Fig. 1c-f and Fig. 2). This enhanced internal oxidation can be attributed to i) preferential adsorption of H_2O [10] as discussed in [41] as well as ii) accelerated oxygen transport at the metal-oxide interfaces in the IOZ discussed above. More research is required to differentiate between these two mechanisms.

5. Conclusions

This paper has presented two important results. First, the austenitization mechanism as main reason for occurrence of internal oxidation in FeCr-base alloys has been experimentally validated via alloying the baseline binary Fe-10Cr alloy with ferrite (Mo) or austenite (Ni) stabilizing elements. At the pO $_2$ level corresponding to the Fe/FeO equilibrium, the transition from internal to external oxidation at 900 $^{\circ}$ C and above is governed predominantly by the alloy microstructure irrespective of the exposure environment, i.e., RP or $\rm H_2/H_2O$: the ferritic lattice (BCC) promotes external scaling of $\rm Cr_2O_3$ while the austenitic (FCC) alloys containing only 10 wt% Cr are prone to internal oxidation.

Second, the classical Wagnerian diffusion analysis was very successful at predicting external oxidation for ferritic Fe-10Cr and internal oxidation for the austenitic alloy. Furthermore, the modeling very accurately predicted the threshold temperature of protectiveness for ferritic Fe-10Cr, i.e., the calculated critical chromium content $N_{Cr}^{crit,1}$

correctly predicted unprotective behavior of the alloy at 1100 °C. At the same time, the supply criterion, $N_{Cr}^{crit,2}$, accurately predicted the amount of Cr-depletion at the oxide-metal interface as well as the effect of the exposure environment, i.e., higher Cr-depletion values for H₂/H₂O than for RP.

Finally, water vapor has been demonstrated to have a limited effect on the transition from protective to unprotective behavior in Fe-10Cr at high temperatures above 900 °C. Although humidity has undoubtedly a measurable detrimental effect on oxidation of Fe-10Cr (deeper IOZs in the $\rm H_2/H_2O$ specimens compared to those exposed in RP), its effect on the total/apparent oxygen permeability (a factor of 1.1–1.2) is much weaker than the effect of austenitization on Cr diffusion (an order of magnitude).

Contributions

All authors contributed to the study conception. The study design, all experiments, material preparation, data collection were performed by AC. The first draft of the manuscript was written by AC. WJQ commended the previous version of the manuscript. All authors read and approved the final manuscript.

CRediT authorship contribution statement

Anton Chyrkin: Writing – review & editing, Writing – original draft, Visualization, Validation, Project administration, Methodology, Investigation, Funding acquisition, Formal analysis, Data curation, Conceptualization. Willem Joseph Quadakkers: Writing – review & editing, Conceptualization.

Declaration of Competing Interest

The authors declare that they have no known competing financial interests or personal relationships that could have appeared to influence the work reported in this paper.

Acknowledgements

This work was funded by the European Union, project MSCA4Ukraine, grant No. 1232975. The present publication reflects only the author's views, and the European Union is not liable for any use that may be made of the information contained therein. Dr. J. Zurek and Dr. D. Naumenko at Forschungszentrum Jülich GmbH, Germany are acknowledged for the chemical analysis of the model alloys.

Data Availability

Data will be made available on a reasonable request.

References

- P. Spätig, J.C. Chen, G.R. Odette, Ferritic and tempered martensitic steels, Struct. Alloy. Nucl. Energy Appl. (2019) 485–527.
- [2] L. Faivre, P.O. Santacreu, A. Acher, A new ferritic stainless steel with improved thermo-mechanical fatigue resistance for exhaust parts, Mater. High. Temp. 30 (2013) 36–42.
- [3] A. Shibli, Boiler steels, damage mechanisms, inspection and life assessment, Power Plant Life Manag. Perform. Improv. (2011) 272–303.
- [4] W.J. Quadakkers, J. Piron-Abellan, V. Shemet, L. Singheiser, Metallic interconnectors for solid oxide fuel cells-a review, Mater. High. Temp. 20 (2003) 115–127.
- [5] S. Chevalier, L. Combemale, I. Popa, et al., Development of SOFC interconnect stainless steels, Solid State Phenom. 300 (2020) 135–156.
- [6] J. Froitzheim, G.H. Meier, L. Niewolak, et al., Development of high strength ferritic steel for interconnect application in SOFCs, J. Power Sources 178 (2008) 163–173.
- [7] Y. Xu, S. Cai, B. Chi, Z. Tu, Technological limitations and recent developments in a solid oxide electrolyzer cell: A review, Int J. Hydrog. Energy 50 (2024) 548–591.
- [8] K. Chen, S.P. Jiang, Review—Materials degradation of solid oxide electrolysis cells, J. Electrochem Soc. 163 (2016) F3070–F3083.

- [9] N.K. Othman, J. Zhang, D.J. Young, Water vapour effects on Fe-Cr alloy oxidation, Oxid. Met. 73 (2010) 337–352.
- [10] J. Ehlers, D.J. Young, E.J. Smaardijk, et al., Enhanced oxidation of the 9%Cr steel P91 in water vapour containing environments, Corros. Sci. 48 (2006) 3428–3454.
- [11] B. Pujilaksono, T. Jonsson, H. Heidari, M. Halvarsson, J.-E. Svensson, L.-G. Johansson, Oxidation of binary FeCr alloys (Fe-2.25Cr, Fe-10Cr, Fe-18Cr and Fe-25Cr) in O₂ and in O₂ + H₂O environment at 600 °C, Oxid. Met. 75 (2011) 183–207.
- [12] J. Chen, J. Zhang, D.J. Young, Effect of hydrogen on oxidation of Fe-20Cr-(1Si, 2Mn or 2Al) alloys in water vapour at 650 °C, Corros. Sci. 251 (2025) 112932.
- [13] J. Wang, S. Mao, J. Zhang, D.J. Young, Effects of Si, Mn, Ti and Ce on oxidation of Fe-Cr alloys in water vapour, npj Mater. Degrad. 9 (1) (2025), 2025;9:1–15.
- [14] E. Essuman, G.H. Meier, J. Zurek, M. Hänsel, W.J. Quadakkers, The effect of water vapor on selective oxidation of Fe-Cr alloys, Oxid. Met. 69 (2008) 143–162.
- [15] N. Mu, K. Jung, N.M. Yanar, et al., The effects of water vapor and hydrogen on the high-temperature oxidation of alloys, Oxid. Met. 79 (2013) 461–472.
- [16] D.J. Young, B.A. Pint, Chromium volatilization rates from Cr₂O₃ scales into flowing gases containing water vapor, Oxid. Met. 66 (2006) 137–153.
- [17] J. Froitzheim, H. Ravash, E. Larsson, L.G. Johansson, J.E. Svensson, Investigation of chromium volatilization from FeCr interconnects by a denuder technique, J. Electrochem Soc. 157 (2010) B1295–B1300.
- [18] H. Asteman, J.E. Svensson, L.G. Johansson, Evidence for chromium evaporation influencing the oxidation of 304L: The effect of temperature and flow rate, Oxid. Met. 57 (2002) 193–216.
- [19] H. Asteman, K. Segerdahl, J.E. Svensson, et al., Oxidation of stainless steel in H₂O/O₂ environments role of chromium evaporation, in: P. Steinmetz, I.G. Wright, G. Meier, A. Galerie, B. Pieraggi, R. Podor (Eds.), High Temperature Corrosion and Protection of Materials 6, 461–464, Prt 1 and 2, Proceedings, 2004, pp. 775–782.
- [20] G.R. Holcomb, Calculation of reactive-evaporation rates of chromia, Oxid. Met. 69 (2008) 163–180.
- [21] A. Galerie, J.P. Petit, Y. Wouters, J. Mougin, A. Srisrual, P.Y. Hou, Water vapour effects on the oxidation of chromia-forming alloys, Mater. Sci. Forum 696 (2011) 200–205.
- [22] D.J. Young, Effects of water vapour on the oxidation of chromia formers, Mater. Sci. Forum (2008) 595–598, 1189–1197.
- [23] T.D. Nguyen, J. Zhang, D.J. Young, Effects of H₂ on microstructures of Cr2O3 scales grown in water vapour and consequences for breakaway, Corros. Sci. 236 (2024) 112265.
- [24] A. Rahmel, Tobolski J. Einfluss von Wasserdampf und Kohlendioxyd auf die Oxydation von Nickel in Sauerstoff bei hohen Temperaturen, Corros. Sci. 5 (1965) 815–820.
- [25] T. Norby, Protonic defects in oxides and their possible role in high temperature oxidation, Le. J. De. Phys. IV 03 (C9) (1993) 99–C9-106.
- [26] B. Tveten, G. Hultquist, T. Norby, Hydrogen in chromium: Influence on the high-temperature oxidation kinetics in O₂, oxide-growth mechanisms, and scale adherence, Oxid. Met. 51 (1999) 221–233.
- [27] M. Schütze, D. Renusch, M. Schorr, Parameters determining the breakaway oxidation behaviour of ferritic martensitic 9%Cr steels in environments containing H₂O, Corros. Eng. Sci. Technol. 39 (2004) 157–166.
- [28] E. Essuman, G.H. Meier, J. Zurek, M. Hänsel, L. Singheiser, W.J. Quadakkers, Enhanced internal oxidation as reason for breakdown of protective chromia scales on FeCr-alloys in water vapour containing gases, High. Temp. Corros. Prot. Mater. 7 Pts 1 2 (2008) 595–598. 699–706.
- [29] E. Essuman, G.H. Meier, J. Zurek, M. Hänsel, L. Singheiser, W.J. Quadakkers, Enhanced internal oxidation as trigger for breakaway oxidation of Fe-Cr alloys in gases containing water vapor, Scr. Mater. 57 (2007) 845–848.
- [30] K.O. Gunduz, A. Chyrkin, C. Goebel, et al., The effect of hydrogen on the breakdown of the protective oxide scale in solid oxide fuel cell interconnects, Corros. Sci. 179 (2021) 109112.
- [31] A. Chyrkin, K.O. Gunduz, V. Asokan, J.-E. Svensson, J. Froitzheim, High temperature oxidation of AISI 441 in simulated solid oxide fuel cell anode side conditions, Corros. Sci. 203 (2022) 110338.
- [32] M.H.Bin Ani, T. Kodama, M. Ueda, K. Kawamura, T. Maruyama, The effect of water vapor on high temperature oxidation of Fe-Cr alloys at 1073 K, Mater. Trans. 50 (2009) 2656–2663.
- [33] A.R. Setiawan, M. Hanafi Bin Ani, M. Ueda, K. Kawamura, T. Maruyama, Oxygen permeability through internal oxidation zone in Fe-Cr alloys under dry and humid conditions at 973 and 1073 K, ISIJ Int. 50 (2010) 259–263.
- [34] D. Jullian, A. Prillieux, J. Zhang, D.J. Young, Oxygen permeability of Fe-Ni-Cr alloys at 1100 and 1150 °C under carbon-free and carbon-containing gases, Mater. Corros. 68 (2017) 197–204.
- [35] A. Prillieux, D. Jullian, J. Zhang, D. Monceau, D.J. Young, Internal oxidation in dry and wet conditions for oxygen permeability of Fe–Ni alloys at 1150 and 1100 °C, Oxid. Met. 87 (2017) 273–283.
- [36] D. Jullian, A. Prillieux, D.B. Hibbert, J. Zhang, D.J. Young, Internal oxidation of austenitic Fe-Ni-Cr alloys at high temperatures: Deduction of oxygen permeability and the influence of carbon-bearing gases, Corros. Sci. 224 (2023) 111465.
- [37] D. Jullian, J. Zhang, D.B. Hibbert, D.J. Young, Oxygen solubility in austenitic Fe-Ni alloys at high temperatures, J. Alloy. Compd. 732 (2018) 646–654.
- [38] V. Shemet, M. Hänsel, Does hydrogen affect oxygen permeability in alloys? Mater. Lett. 172 (2016) 6–10.
- [39] A. Chyrkin, C. Cossu, J.-E. Svensson, J. Froitzheim, Internal oxidation of a Fe-Cr binary alloy at 700-900 °C: the role of hydrogen and water vapor, Oxid. Met. 98 (2022) 273-289.

- [40] A. Chyrkin, C. Cossu, J.-E. Svensson, J. Froitzheim, Effect of hydrogen on the internal oxidation of a Pd-Cr Alloy in dual-atmosphere conditions, Oxid. Met. 97 (2022) 527–538.
- [41] A. Chyrkin, J. Froitzheim, W.J. Quadakkers, Transition from internal to external oxidation in binary Fe–Cr alloys around 900 °C, High. Temp. Corros. Mater. 102 (2025) 1–22.
- [42] F. Rhines, W. Johnson, W. Anderson, Rates of high-temperature oxidation of dilute copper alloys, Trans. Metall. Soc. Aime. 147 (1942) 205–221.
- [43] J. Zurek, G.H. Meier, E. Wessel, L. Singheiser, W.J. Quadakkers, Temperature and gas composition dependence of internal oxidation kinetics of an Fe-10%Cr alloy in water vapour containing environments, Mater. Corros. 62 (2011) 504–513.
- [44] A.F. Guillermet, andez. The Fe-Mo (Iron-Molybdenum) system, Bull. Alloy Phase Diagr. 3 (1982) 359–367.
- [45] A. Jacob, E. Povoden-Karadeniz, E. Kozeschnik, Revised thermodynamic description of the Fe-Cr system based on an improved sublattice model of the σ phase, Calphad 60 (2018) 16–28.
- [46] C. Wagner, Reaktionstypen bei der Oxydation von Legierungen, Z. fur Elektrochem. 63 (1959) 772–790.
- [47] C. Wagner, Oxidation of alloys involving noble metals, J. Electrochem Soc. 103 (1956) 571.
- [48] Thermo-Calc. TCFE6 TCS Steels/Fe-Alloys Database Version 6 (2) (2013).
- [49] C. Wagner, Theoretical Analysis of the diffusion processes determining the oxidation rate of alloys, J. Electrochem Soc. 99 (1952) 369.
- [50] E. Essuman, G.H. Meier, J. Zurek, et al., Protective and non-protective scale formation of NiCr alloys in water vapour containing high- and low-pO₂ gases, Corros. Sci. 50 (2008) 1753–1760.
- [51] G.H. Meier, K. Jung, N. Mu, et al., Effect of alloy composition and exposure conditions on the selective oxidation behavior of ferritic Fe-Cr and Fe-Cr-X alloys, Oxid. Met. 74 (2010) 319–340.
- [52] R.A. Rapp, The transition from internal to external oxidation and the formation of interruption bands in silver-indium alloys, Acta Metall. 9 (1961) 730–741.
- [53] J.H. Swisher, E.T. Turkdogan, Solubility, permeability and diffusivity of oxygen in solid iron, Trans. Metall. Soc. Aime. 239 (1967) 426–431.
- [54] D.P. Whittle, G.C. Wood, D.J. Evans, D.B. Scully, Concentration profiles in the underlying alloy during the oxidation of iron-chromium alloys, Acta Metall. 15 (1967) 1747–1755.
- [55] P.I. Williams, R.G. Faulkner, Chemical volume diffusion coefficients for stainless steel corrosion studies, J. Mater. Sci. 22 (1987) 3537–3542.
- [56] W. Gordon, A. Van Bennekom, Review of stabilisation of ferritic stainless steels, Mater. Sci. Technol. 12 (1996) 126–131.
- [57] J.E. Croll, G.R. Wallwork, The design of iron-chromium-nickel alloys for use at high temperatures, Oxid. Met. 1 (1) (1969) 55–71, 1969;1.
- [58] J. Pirón Abellán, T. Olszewski, H.J. Penkalla, G.H. Meier, L. Singheiser, W. J. Quadakkers, Scale formation mechanisms of martensitic steels in high CO₂/H₂O-containing gases simulating oxyfuel environments, Mater. High. Temp. 26 (2009) 63–72.
- [59] P. Huczkowski, A. Chyrkin, L. Singheiser, W. Nowak, W.J. Quadakkers, Corrosion behavior of candidate heat exchanger materials in oxidizing and reducing gases, relevant to oxyfuel combustion, in: International Corrosion Conference Series, 3, NACE, 2016.
- [60] G.R. Holcomb, Steam oxidation and chromia evaporation in ultrasupercritical steam boilers and turbines, J. Electrochem Soc. 156 (2009) C292–C297.
- [61] T.S. Gendron, P.M. Scott, S.M. Bruemmer, L.E. Thomas, Internal oxidation as a mechanism for steam generator tube degradation, Proc. Third Int. Conf. Steam. Gener. Heat. Exch. Tor. Can. (1998).
- [62] J. Zurek, E. Wessel, L. Niewolak, et al., Anomalous temperature dependence of oxidation kinetics during steam oxidation of ferritic steels in the temperature range 550-650 °C, Corros. Sci. 46 (2004) 2301–2317.
- [63] D.J. Young, J. Zurek, L. Singheiser, W.J. Quadakkers, Temperature dependence of oxide scale formation on high-Cr ferritic steels in Ar-H₂-H₂O, Corros. Sci. 53 (2011) 2131–2141
- [64] A. Chyrkin, J. Froitzheim, J. Zurek, D. Naumenko, Austenitization triggering breakaway oxidation of FeCr-base alloys at 900 °C, Corros. Sci. 244 (2025) 112605.
- [65] G.R. Holcomb, M. Ziomek-Horoz, S.D. Cramer, B.S. Covino, S.J. Bullard, Dualenvironment effects on the oxidation of metallic interconnects, J. Mater. Eng. Perform. 15 (2006) 404–409.
- [66] P. Alnegren, M. Sattari, J.E. Svensson, J. Froitzheim, Severe dual atmosphere effect at 600 °c for stainless steel 441, J. Power Sources 301 (2016) 170–178.
- [67] K. Nakagawa, Y. Matsunaga, T. Yanagisawa, Corrosion behavior of ferritic steels on the air sides of boiler tubes in a steam/air dual environment, Mater. High. Temp. 18 (2001) 51–56.
- [68] K. Chandra, A. Kranzmann, High temperature oxidation of 9–12% Cr ferritic/martensitic steels under dual-environment conditions, Corros. Eng. Sci. Technol. 53 (2018) 27–33.
- [69] M. Stanislowski, J. Froitzheim, L. Niewolak, et al., Reduction of chromium vaporization from SOFC interconnectors by highly effective coatings, J. Power Sources 164 (2007) 578–589.
- [70] M.J. Reddy, T.E. Chausson, J.E. Svensson, J. Froitzheim, 11–23% Cr steels for solid oxide fuel cell interconnect applications at 800 °C – How the coating determines oxidation kinetics, Int J. Hydrog. Energy 48 (2023) 12893–12904.
- [71] H. Falk-Windisch, J. Claquesin, M. Sattari, J.E. Svensson, J. Froitzheim, Co- and Ce/Co-coated ferritic stainless steel as interconnect material for Intermediate Temperature Solid Oxide Fuel Cells, J. Power Sources 343 (2017) 1–10.

- [72] F.H. Stott, Y. Shida, D.P. Whittle, G.C. Wood, B.D. Bastow, The morphological and structural development of internal oxides in nickel-aluminum alloys at high temperatures, Oxid. Met. 18 (1982) 127–146.
- [73] A. Martínez-Villafañe, F.H. Stott, J.G. Chacon-Nava, G.C. Wood, Enhanced oxygen diffusion along internal oxide-metal matrix interfaces in Ni-Al alloys during internal oxidation, Oxid. Met. 57 (2002) 267–279.
- [74] H. Hindam, D.P. Whittle, High temperature internal oxidation behaviour of dilute Ni-Al alloys, J. Mater. Sci. 18 (1983) 1389–1404.
- [75] W. Zhao, B. Gleeson, Assessment of the detrimental effects of steam on $\rm Al_2O_3$ -scale establishment, Oxid. Met. 83 (2015) 607–627.
- [76] W. Zhao, Y. Kang, J.M.A. Orozco, B. Gleeson, Quantitative approach for determining the critical volume fraction for the transition from internal to external oxidation, Oxid. Met. 83 (2015) 187–201.
- [77] I. Barin, F. Sauert, E. Schultze-Rhonhof, W.S. Sheng, Thermochemical data of pure substances, Part 1, Ag-Kr, VCH, 1993.